^{177}Lu-DOTA-EB-TATE, a Radiolabeled Analogue of Somatostatin Receptor Type 2, for the Imaging and Treatment of Thyroid Cancer

Shilpa Thakur[1], Brianna Daley[1], Corina Millo[2], Craig Cochran[1], Orit Jacobson[3], Huiyan Lu[4], Zhantong Wang[5], Dale Kiesewetter[3], Xiaoyuan Chen[5], Vasyl Vasko[6], and Joanna Klubo-Gwiezdzinska[1]

ABSTRACT

Purpose: The goal of this study was to analyze the role of somatostatin receptor type 2 (SSTR2) as a molecular target for the imaging and treatment of thyroid cancer through analysis of SSTR2 expression and its epigenetic modulation and testing tumor uptake of different radiolabeled SSTR2 analogues.

Experimental Design: We analyzed SSTR2 expression by immunostaining of 92 thyroid cancer tissue samples and quantified standard uptake values (SUV_{max}) of SSTR2 analogue, ^{68}Ga-DOTA-TATE, by PET/CT imaging in 25 patients with metastatic thyroid cancer. We utilized human thyroid cancer cell lines characterized by differential SSTR2 expression (TT, BCPAP, and FTC133) and rat pancreatic cell line (AR42J) with intrinsically high SSTR2 expression for functional *in vitro* studies. SSTR2-high (AR42J) and SSTR2-low (FTC133) xenograft mouse models were used to test the uptake of radiolabeled SSTR2 analogues and their therapeutic efficacy *in vivo*.

Results: Thyroid cancer had a higher SSTR2 expression than normal thyroid. Hurthle cell thyroid cancer was characterized by the highest ^{68}Ga-DOTA-TATE uptake [median SUV_{max}, 16.5 (7.9–29)] than other types of thyroid cancers. *In vivo* studies demonstrated that radiolabeled DOTA-EB-TATE is characterized by significantly higher tumor uptake than DOTA-TATE ($P < 0.001$) and DOTA-JR11 ($P < 0.001$). Treatment with ^{177}Lu-DOTA-EB-TATE extended survival and reduced tumor size in a mouse model characterized by high somatostatin (SST) analogues uptake (SUV_{max}, 15.16 $\pm$ 4.34), but had no effects in a model with low SST analogues uptake (SUV_{max}, 4.8 $\pm$ 0.27).

Conclusions: A novel SST analogue, ^{177}Lu-DOTA-EB-TATE, has the potential to be translated from bench to bedside for the targeted therapy of patients characterized by high uptake of SST analogues in metastatic lesions.

Introduction

The current treatment regimen for metastatic differentiated thyroid cancer (DTC) includes thyroidectomy followed by radioactive iodine (RAI) therapy, while medullary thyroid cancer (MTC) is routinely treated with surgery and tyrosine kinase inhibitors (1). Unfortunately, 5%–22% of patients become refractory to standard therapy, particularly patients with Hurthle cell thyroid cancer (HTC), characterized by low RAI uptake in metastatic lesions (2, 3). Previous studies have reported that the average survival for patients with RAI-refractory DTC is around 2.5–3.5 years and with aggressive metastatic MTC even shorter, 1.75 years (4–6). There is a clear need for improved therapy in these patients.

Somatostatins (SST) are a family of cyclopeptides that are produced by endocrine, gastrointestinal, neuronal, and immune cells (7). The metabolically stable SST analogues have been labeled with radionuclides to utilize them in peptide receptor radionuclide therapy (PRRT; ref. 8). Treatment efficacy depends on the expression of SST receptors, among which somatostatin receptor type 2 (SSTR2) is the most commonly expressed on tumor tissues (9). Currently, there are several SST analogues available with varying SSTR2 affinities and tumor retention time, with only two (radiolabeled DOTA-TATE and DOTA-TOC) currently approved by the FDA for the imaging of neuroendocrine tumors (10, 11) and one approved for the treatment of gastroenteropancreatic neuroendocrine tumors, lutetium (^{177}Lu)-labeled DOTA-TATE (12). Moreover, recent studies have shown that an SSTR2 agonist combined with Evans blue analogue (DOTA-EB-TATE) is characterized by a higher tumor uptake and residence time *in vivo* in preclinical models and in pilot studies of patients with advanced metastatic neuroendocrine tumors (13, 14). Recently synthesized SSTR2 antagonists, such as JR11, although not internalized, are reported to have superior binding affinity and long residence time due to slow dissociation from the receptor (15). JR11 was reported to exert superior binding characteristics and tumor-to-background uptake ratios in preclinical models and in pilot clinical trials in patients with metastatic neuroendocrine tumors (16–18).

Interestingly, the NIH case series of patients with neuroendocrine tumors revealed incidental uptake of radiolabeled SST analogue, ^{68}Gallium- (^{68}Ga)-DOTA-TATE, in thyroid nodules, among which 21% were found to be malignant (19). However, there are no data on the role of radiolabeled DOTA-EB-TATE and DOTA-JR11 in the diagnosis and treatment of thyroid cancer. Therefore, the goal of this study was to provide a comprehensive analysis of

[1]Metabolic Disease Branch, National Institute of Diabetes and Digestive and Kidney Diseases, NIH, Bethesda, Maryland. [2]Clinical Center, NIH, Bethesda, Maryland. [3]Molecular Tracer and Imaging Core Facility, National Institute of Biomedical Imaging and Bioengineering, NIH, Bethesda, Maryland. [4]National Institute of Diabetes and Digestive and Kidney Diseases, NIH, Bethesda, Maryland. [5]Laboratory of Molecular Imaging and Nanomedicine, National Institute of Biomedical Imaging and Bioengineering, NIH, Bethesda, Maryland. [6]Department of Pediatric Endocrinology, Uniformed Services of the Health Sciences, Bethesda, Maryland.

Note: Supplementary data for this article are available at Clinical Cancer Research Online (http://clincancerres.aacrjournals.org/).

Corresponding Author: Joanna Klubo-Gwiezdzinska, National Institute of Diabetes and Digestive and Kidney Diseases, NIH, Bethesda, MD 20892. Phone: 240-688-3589; E-mail: joanna.klubo-gwiezdzinska@nih.gov

Clin Cancer Res 2021;27:1399–409

doi: 10.1158/1078-0432.CCR-20-3453

Translational Relevance

We demonstrated that somatostatin receptor type 2 (SSTR2) may serve as a molecular target in the diagnosis and treatment of a subset of patients with thyroid cancer. We showed that thyroid cancer lesions have higher SSTR2 expression than normal thyroid. Furthermore, we reported high uptake of somatostatin (SST) analogue, ^{68}Ga-DOTA-TATE, in a subset of patients with thyroid cancer, particularly in Hurthle cell thyroid cancer (HTC) resistant to standard treatment. *In vivo* studies demonstrated that the theranostic efficacy of SST analogues could be enhanced by utilizing radiolabeled DOTA-EB-TATE, which is characterized by significantly higher tumor uptake than DOTA-TATE and DOTA-JR11. Treatment with ^{177}Lu-DOTA-EB-TATE extended survival and reduced tumor size in a mouse model with high SST analogue uptake, comparable with the uptake observed in human HTC. Overall, ^{177}Lu-DOTA-EB-TATE has the potential to be translated from bench to bedside for the targeted therapy of patients with thyroid cancer characterized by high tumor uptake of SST analogues.

SSTR2 expression and mechanisms of its upregulation in thyroid cancer and compare the uptake and therapeutic efficacy of radiolabeled SST analogues, which are characterized by different binding capacity and tumor retention times in preclinical models of SSTR2-positive tumors.

Materials and Methods

Analysis of ^{68}Ga-DOTA-TATE uptake in patients with metastatic thyroid cancer

The protocol for human studies was approved by the NIH Institutional Review Board (Bethesda, MD) and Radiation Safety Committee. All patients gave written informed consent to participate in the studies that were conducted in accordance with the ethical guidelines outlined in the Declaration of Helsinki, CIOMS, Belmont Report, and U.S. Common Rule. We performed a pilot clinical trial (clinicaltrials.gov identifier ID: NCT00001160) aimed at screening patients with RAI non-avid metastatic DTC and MTC for the presence of SSTR2 expression by imaging with ^{68}Ga-DOTA-TATE PET/CT. Each patient received 5 mCi of ^{68}Ga-DOTA-TATE intravenously followed by PET/CT imaging per standard protocol. Any lesion demonstrating activity higher than the physiologic uptake of the involved organ was considered a "true" lesion, unless correlative anatomic imaging suggested nonmalignant or alternative pathology (20). Two investigators (C. Millo and J. Klubo-Gwiezdzinska) analyzed the images and obtained maximum and mean standard uptake values (SUV) for up to six lesions in each patient.

Cell culture

The human thyroid cancer cell lines gifted from Dr. Electron Kebebew (Stanford University, Stanford, CA) or purchased from University of Colorado Cancer Center (Aurora, CO) or the ATCC were used in this study: follicular thyroid cancer, FTC133; papillary thyroid cancer, BCPAP and TPC1; MTC, TT; anaplastic thyroid cancer, THJ16T, THJ29T, 8505C, OCUT2, KAT18, SW1736, and C643 (ATC); and HTC, XTC1. A rat pancreatic cell line, AR42J, with intrinsically high SSTR2 expression, was used as a positive control for SST analogue uptake studies (13). The cells were authenticated by short tandem repeat analysis and contamination was excluded via IMPACT II PCR analysis.

The cells were grown in the standard media, supplemented with 10% FBS (Thermo Fisher Scientific) for human cell lines and 20% for a rat AR42J cell line, as well as with 10 U/mL Penicillin–Streptomycin (Gibco) and 0.25 μg/mL Amphotericin B (Gibco). For treatment (72 hours), valproic acid (Sigma-Aldrich, PHR1061) was added to the culture medium at a final concentration of 2 or 4 mmol/L, while tacedinaline (Sigma-Aldrich, C0621) and decitabine (Sigma-Aldrich, A3656) were added at final concentration of 500 and 75 ng/mL, respectively, which corresponds to their therapeutic serum concentrations (21).

RNA extraction and real-time reverse-transcription PCR

For mRNA analysis, cells were seeded in 6-well plates and total RNA was isolated from the cells using RNeasy Mini Kit (Qiagen). RNA was quantified using Nanodrop (manufacturer) and 1 μg of RNA was used to synthesize cDNA using the iScript cDNA Synthesis Kit (Bio-Rad). The relative gene expression was analyzed using iQ SYBR Green SuperMix (Bio-Rad) on a StepOnePlus Real-Time PCR Detection System (Applied Biosystems). We used commercially available primers for the analysis of *SSTR2* (Hs_SSTR2_1_SG QuantiTect primer assay and Rn_Sstr2_1_SG QuantiTect primer assay) and *β-actin* (Hs_ACTB_2_SG QuantiTect primer assay and Rn_Actb_1_SG QuantiTect primer assay) expression. The relative gene expression was normalized to β-actin and calculated using the $2^{-\Delta\Delta C_t}$ method.

Western blotting

Cells were seeded in a 10-cm culture plate and lysed using Mammalian Protein Extraction Reagent (M-PER, Thermo Fisher Scientific) as per the manufacturer's instructions. To increase the protein concentration, Amicon Centrifugal Filters (Millipore) were used. The protein concentration was determined by using the DC protein assay kit II. The samples were loaded onto 4%–12% SDS-PAGE Gel (Novex; 30–50 μg/lane) and transferred onto a polyvinylidene difluoride membrane using a Trans-blot Turbo System (Bio-Rad). The membranes were blocked with 3% BSA and prepared in PBST for 1 hour at room temperature. The membranes were incubated overnight at 4°C with a primary antibody against SSTR2 (1:400, R&D Systems, MAB4224), acetylated histone 3 (1:500, Millipore, 06-599), or acetylated histone 4 (1:500, Millipore, 06-598), GAPDH (1:1,000; Invitrogen, MA5-15738), and β-actin (1:1,000, Santa Cruz Biotechnology, sc-47778). The membranes were washed three times with PBST followed by incubation with either anti-mouse or anti-rabbit secondary antibody for 1 hour at room temperature. The membranes were finally washed three times with PBST and imaged using ECL (Azure Biosystems) and an Imaging System (Bio-Rad).

Cell surface expression of SSTR2

To analyze the membranous expression of SSTR2, cells were harvested, washed, and counted. The cells were then resuspended in ice-cold PBS containing 10% FCS and 1% sodium azide at a concentration of 2×10^6 cells/mL. For each sample, 200 μL of this cell suspension was used and 2 μg of SSTR2 antibody was added and incubated for 1 hour at room temperature. Following incubation, the cells were washed three times with ice-cold PBS by centrifugation at 1,000 rpm for 5 minutes. After washings, cells were incubated with an Alexa Fluor 680–labeled secondary antibody (4 μg), which was prepared in 3% BSA in PBS. The cells were incubated for 30 minutes at room temperature in the dark and washed three times, followed by resuspension in ice-cold PBS containing 3% BSA and 1% sodium azide.

The cells were immediately analyzed by Flow Cytometer (LSR II, BD Biosciences) for SSTR2 membranous expression. To avoid any detection of intracellular SSTR2, cell permeabilization was avoided.

IHC

Immunostaining was performed on commercially available Human Thyroid Cancer Tissue Microarray Slides (US Biomax Inc.), on formalin-fixed, paraffin-embedded tissue samples from thyroidectomized patients (MTC and HTC), and animal thyroid cancer models. Sections were dewaxed, soaked in alcohol, and then microwave treated in Antigen Unmasking Solution (Vector Laboratories) for 10 minutes. Endogenous peroxidase activity was quenched by incubation in 3% hydrogen peroxide. Sections were then incubated for 10 minutes in a working solution of blocking serum and incubated at 4°C overnight with anti-SSTR2 antibody (Abcam, catalog no., ab9550, dilution 1/100). Immunostaining was performed using the Vectastain Universal Quick Kit (Vector Laboratories Inc.) as per the manufacturer's instructions. Sections were incubated with biotinylated secondary antibody for 10 minutes and in streptavidin/peroxidase complex working solution for 10 minutes. Peroxidase staining was revealed with the ImmPact DAB Peroxidase Substrate Kit (Vector Laboratories). Sections were counterstained with hematoxylin and mounted. The antiserum was omitted in the negative control. The results of staining were interpreted and scored independently by two investigators (V. Vasko and J. Klubo-Gwiezdzinska). The intensity of staining was scored as 0 (negative staining) and 1 (positive, intensity similar to those obtained in positive control). The quantitative data from the assessment of relative percentage of immunopositive cells in thyroid tissue samples were calculated as 0, no staining; 1, positive staining in <25% of cells; 2, positive staining in 25%–50% of cells; and 3, positive staining in >50% of cells. The final immunoscore was calculated by multiplying each score (22).

Chromatin immunoprecipitation assay

Cells were cultured in 150-mm cell culture dishes. The chromatin immunoprecipitation (ChIP) assay was performed using the ChIP-IT Express Enzymatic Kit (Active Motif, 53009) as per the manufacturer's instructions. The chromatin was sheared using the ChIP-IT Express Enzymatic Kit (Active Motif, 53035). We used Histone H3ac (pan-acetyl) antibody (Active Motif, 39139), Histone H4ac (pan-acetyl) antibody (Active Motif, 39243), and isotype IgG control for immunoprecipitation. The immunoprecipitated DNA was analyzed by real-time PCR for H3 and H4 acetylation at the SSTR2 promoter by using primers directed against the human and rat *SSTR2* gene promoter. The sequences of human SSTR2 primers are: forward primer, GAAGGAAGGAAGGAAGAA and reverse primer, GGATGAAGTCATTGATGTC, while the sequences of rat SSTR2 primers are: forward primer, CCCGGGACTGGTCCGTGGTA and reverse primer, CAGCTGGTGTGGCGACTGGG. ChIP data were normalized to the input DNA and analyzed as fold enrichment relative to isotype control antibody.

Mice models

The animal protocol for the experiments was approved by the NIDDK Animal Care and Use Committee. Eight- to 10-week-old athymic nude mice and NOD.Cg-Prkdcscid Il2rgtm1Wjl/SzJ mice (The Jackson Laboratory) were used to create subcutaneous xenograft and metastatic mouse models, respectively. For the metastatic model, the mice received a tail vein injection of FTC133 (16×10^4 cells) containing a linearized pGL4.51[luc2/CMV/Neo] vector (23). The tumor burden was monitored weekly in the mice using the IVIS Lumina *In Vivo* Imaging System (PerkinElmer) by injecting them with luciferin (150 mg luciferin/kg body weight, PerkinElmer) 10 minutes before imaging. For the subcutaneous xenograft model, athymic nude mice were injected subcutaneously with FTC133, BCPAP, TT, or AR42J (5×10^5 cells). The tumor burden was monitored regularly by using a Vernier caliper. The mice were euthanized if the tumors exceeded 2 cm in diameter, impeded movement, or if there were signs of breathing difficulty at any point in the study. The mice were grouped into control and treatment groups based on weight, gender, and tumor burden. The mice were then treated with either valproic acid (300 μg/kg, Sigma-Aldrich, P4543), decitabine (1 mg/kg), or saline (placebo) via intraperitoneal injections daily for 10 days followed by PET imaging or radionuclide therapy studies (Supplementary Fig. S8).

PET imaging and biodistribution studies

PET imaging was performed in the metastatic mice model at 4–5 weeks after inoculation when the average luminescence in the metastatic areas was in the range of 10^7–10^8. For the subcutaneous xenograft mice model, PET imaging was performed when the tumor size exceeded 1 cm. The FTC133 and AR42J formed 1–2 cm tumors within 2 weeks after inoculation, while BCPAP in 3–4 weeks and TT in 4–5 weeks. Each mouse received a dose of approximately 100 μCi of each radiolabeled SST analogue (^{68}Ga-DOTA-TATE, ^{68}Ga-DOTA-JR11, and ^{86}Y-DOTA-EB-TATE) consecutively via tail vein injection. DOTA-TATE (TATE supplied by CSBio) and DOTA-JR11 (JR11 provided by IPSEN), as agents characterized by a short half-life, were labeled with ^{68}Ga with a half-life of 67.7 minutes. DOTA-EB-TATE (EB-TATE patented by NIH and licensed by Molecular Targeting Technologies Inc.), an agent with a long half-life in the blood due to a reversible binding to albumin[25], required radiolabeling with ^{86}Y, because this isotope is characterized by a longer half-life of 14.7 hours. These pharmacokinetics and pharmacodynamics formed the rationale for the particular order of consecutive injections for each mouse with ^{68}Ga-DOTA-TATE and ^{68}Ga-DOTA-JR11, injected 4 hours apart (∼4 half-lives apart), followed by DOTA-EB-TATE as the last SST analogue in all mice (Supplementary Fig. S8A). Randomization to injection of the DOTA-EB-TATE as the first agent is futile because it would necessitate performing the remaining PET/CTs after approximately 4 days (∼4 half-lives). Significant tumor growth could take place during this delay, rendering the imaging results incomparable. The static PET imaging for ^{68}Ga-DOTA-TATE and ^{68}Ga-DOTA-JR11 was done at 60 minutes postinjection, while for ^{86}Y-DOTA-EB-TATE, imaging was performed at 16–24 hours postinjection, per the previously published pharmacokinetics and pharmacodynamics studies (13, 24). The PET scans were acquired on Inveon (Siemens) scanners. The PET images were analyzed using ASIPro (Siemens) to plot regions of interest and calculate SUV. The SUV was corrected for injected radioactivity dose, decay, branching, and mouse weight. After the last scan, mice were euthanized and tumor, heart, lungs, liver, spleen, and kidneys were collected to perform biodistribution studies. The counts per minute readings were normalized by the weight of the tissues and biodistribution data are presented as percentages of the injected dose per gram of tissue (%ID/g).

PRRT

To evaluate therapeutic efficacy, the SST analogues were labeled with the therapeutic radionuclide, ^{177}Lu. The FTC133 and AR42J tumor mice models were pretreated with either placebo or valproic acid, with a goal of inducing SSTR2 expression in the tumors of

valproic acid–treated animals. The mice were divided into control and valproic acid groups based on their body weight and gender. Two weeks after inoculation, the mice in control and valproic acid groups were subdivided into the following groups: (i) control placebo-treated mice receiving ^{177}Lu-DOTA-EB-TATE (500 μCi), (ii) control placebo-treated mice receiving saline, (iii) valproic acid–treated mice receiving ^{177}Lu-DOTA-EB-TATE (500 μCi), and (iv) valproic acid–treated mice receiving saline (Supplementary Fig. S8B). All mice received two doses of either ^{177}Lu-DOTA-EB-TATE or saline a week apart. The tumor burden in each mouse was monitored twice a week and living mice were euthanized 60 days after first ^{177}Lu-DOTA-EB-TATE injection. The tumor burden was calculated by using the formula: tumor volume = (width^2 × length)/2.

Subsequently, to compare the therapeutic effects of different SST analogues, we utilized mice with AR42J tumors characterized by the highest SST analogues uptake. Prior to therapy initiation, the mice were divided into three groups based on their tumor volume, gender, and body weight as follows: (i) ^{177}Lu-DOTA-TATE (500 μCi), (ii) ^{177}Lu-DOTA-JR11 (500 μCi), and (iii) ^{177}Lu-DOTA-EB-TATE (500 μCi; Supplementary Fig. S8C). All mice received their first dose 2 weeks after inoculation and the second dose was given 7 days later. The effect of the therapy was analyzed by obtaining tumor measurements twice a week. Living mice were euthanized 24 days after first ^{177}Lu-labeled SST analogue injection.

Statistical analysis

GraphPad Prism 8.1 software was used for data analysis. A two-tailed unpaired Student *t* test was used for comparison between two groups. One-way ANOVA with *post hoc* Tukey test was used for comparison between more than two groups. Data are presented as mean ± SD or mean ± SEM for normally distributed data and median with (25–75 interquartile range) for skewed data. $P < 0.05$ was considered significant.

Results

SSTR2 is overexpressed in thyroid cancer compared with normal thyroid tissue

RNA sequencing data available in The Cancer Genome Atlas database were analyzed for 507 patients with papillary thyroid cancer (PTC; ref. 25), demonstrating that *SSTR2* is expressed in all PTC stages and subtypes (Supplementary Fig. S1A and S1B). This included 65 paired samples of tumor versus normal thyroid tissues, derived from the same patients, which demonstrated significantly higher SSTR2 expression in tumor tissue samples compared with the paired normal thyroid tissues (log fold change, 0.6; $P = 0.03$).

Immunostaining on 92 human tissue samples, 84 thyroid cancer tissue samples (39 PTCs, 19 FTCs, 6 poorly differentiated cancers, 16 MTCs, and 4 HTCs) and 8 normal thyroid tissues, showed high SSTR2 protein expression (IHC scores, 2 and 3) in 51.4% (35/68) of thyroid cancer samples of epithelial origin and 43.8% (7/16) of MTC samples. There was no significant expression in the normal thyroid samples (**Fig. 1A**; Supplementary Table S1).

The highest ^{68}Ga-DOTA-TATE uptake is observed in patients with metastatic HTC

To analyze the presence of SSTR2 in thyroid cancer metastases, ^{68}Ga-DOTA-TATE PET/CT was performed in patients with RAI non-avid metastatic DTC and MTC. Among 25 enrolled patients, ages 52.2 ± 13 years old at the study enrollment and 40 ± 15 years old at thyroid cancer diagnosis, 13 of 25 (52%) were females, 5 presented with HTC, 8 with MTC, and 12 with PTC. ^{68}Ga-DOTA-TATE PET/CT was positive in 20 of 25 (80%) patients. The highest uptake was observed in patients with HTC [median SUV_{max}, 16.5 (7.9–29)] compared with patients with MTC, characterized by low-to-moderate SUV_{max} [median, 4.3 (3.2–9.5); $P = 0.019$], and patients with PTC, with median SUV_{max} of 5.4 [(3.8–7.8); $P = 0.007$; **Fig. 1B**]. Two patients with MTC and 3 with PTC had no evident uptake above the background, suggesting a lack of, or very low, SSTR2 expression in their metastatic lesions. The PET/CT images demonstrating high ^{68}Ga-DOTA-TATE uptake are depicted in **Fig. 1C** (HTC), **D** (PTC), and **E** (MTC). Because the high therapeutic efficacy of PRRT in neuroendocrine tumors has been associated with tumors characterized by $SUV_{max} > 13$–15 (26, 27), we further showed that $SUV_{max} > 15$ was observed in at least one metastatic lesion in 7 of 25 (28%) enrolled patients. It was observed in 4 of 5 (80%) patients with metastatic HTC, 1 of 12 (8.3%) patients with metastatic PTC, and 2 of 8 (25%) patients with metastatic MTC (Supplementary Table S2).

Given only low-to-moderate ^{68}Ga-DOTA-TATE uptake in a majority of patients with PTC and MTC, functional *in vitro* and *in vivo* studies were performed to test whether SSTR2 expression could be significantly and safely upregulated and whether radiolabeled SST analogues, besides DOTA-TATE, might be associated with higher tumor uptake.

Thyroid cancer cell lines are characterized by variable SSTR2 expression that can be epigenetically upregulated

Several thyroid cancer cell lines were screened for the presence of *SSTR2* by RT-PCR (Supplementary Fig. S1C). The thyroid cancer cell lines, TT, FTC133, and BCPAP, were chosen for subsequent functional *in vitro* and *in vivo* studies based on differential SSTR2 expression, histologic origin, and ability to form tumors *in vivo* (Supplementary Fig. S1E).

Because the thyroid cancer cell lines had low-to-moderate SSTR2 expression, it was analyzed whether SSTR2 could be upregulated in an *in vitro* model. *SSTR2* is an epigenetically regulated gene and, therefore, we utilized epigenetic modifiers, histone deacetylase (HDAC) inhibitors, valproic acid and tacedinaline, and DNA methyltransferase inhibitor, decitabine (21). Valproic acid was observed to be a more potent inducer of SSTR2 expression in thyroid cancer cells in comparison with tacedinaline and decitabine (Supplementary Fig. S2A and S2B). Treatment with 2 or 4 mmol/L valproic acid for 72 hours significantly upregulated SSTR2 expression in FTC133, BCPAP, and TT cells (**Fig. 2A–C**, and **F–H**; Supplementary Fig. S1F–S1I and S1K), as well as in the AR42J cell line (**Fig. 2K–M**; Supplementary Fig. S1J). Flow cytometry demonstrated an increased membranous SSTR2 expression in examined cell lines (**Fig. 2B**, **G**, and **L**). Valproic acid treatment resulted in growth inhibition by promoting cell-cycle arrest (Supplementary Fig. S3A–S3L).

Because valproic acid is an HDAC inhibitor, the effects of valproic acid on the acetylation of histones 3 (H3ac) and 4 (H4ac) were analyzed. As indicated in **Fig. 2D**, **I**, and **N**, we observed an increase in H3ac and H4ac in valproic acid–treated FTC133, BCPAP, and AR42J cells. To further identify whether valproic acid–mediated upregulation of *SSTR2* expression is caused by an increase in H3ac or H4ac at the *SSTR2* promoter, ChIP assays were performed. Valproic acid treatment in BCPAP and AR42J cells resulted in a significant increase in both H3ac (1.9-fold BCPAP; $P < 0.001$ and 2.8-fold AR42J; $P < 0.001$) and H4ac (2.9-fold BCPAP; $P < 0.001$ and 2.7-fold AR42J; $P < 0.01$; **Fig. 2J** and **O**). In contrast, in FTC133 cells, H4ac was increased by 2.4-fold ($P < 0.001$) at the *SSTR2* promoter, while H3ac was slightly, but significantly reduced ($P < 0.05$; **Fig. 2E**). Overall, our

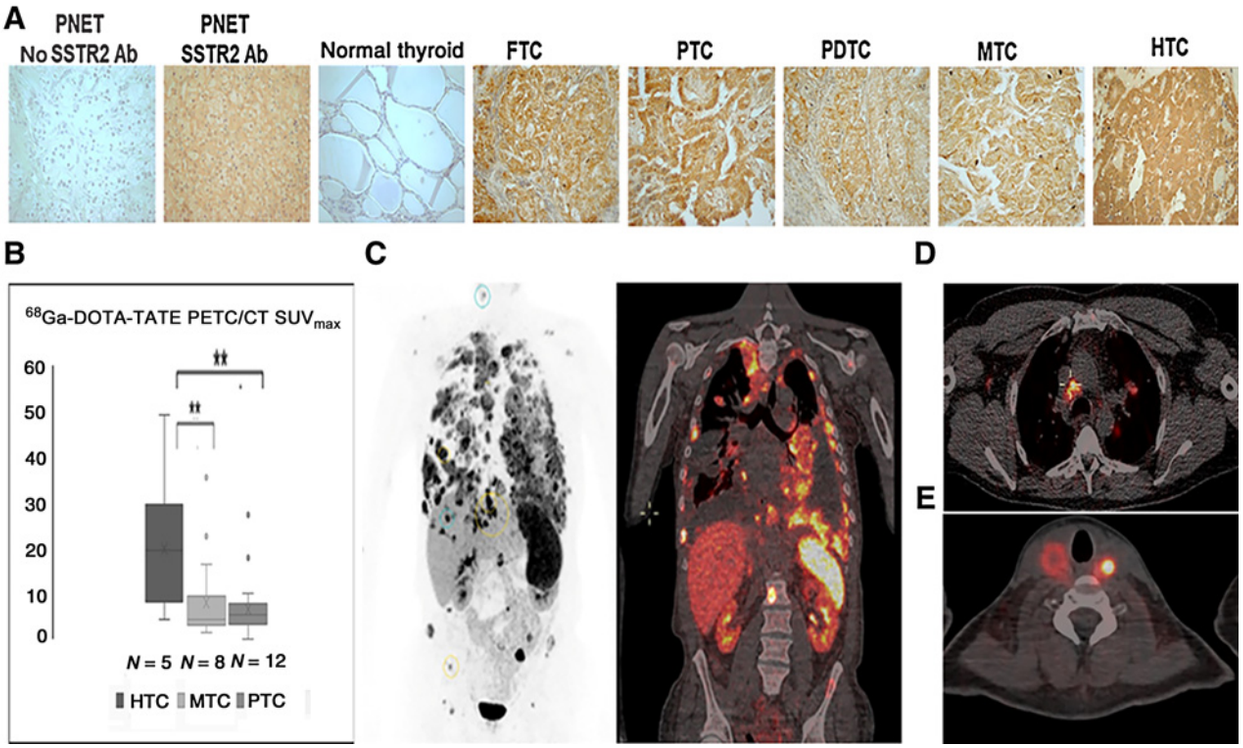

Figure 1.

A subset of patients with thyroid cancer is characterized by moderate-to-high ^{68}Ga-DOTA-TATE uptake. **A,** Representative images showing increased expression of SSTR2 in thyroid cancer compared with normal thyroid, documented by immunostaining (Supplementary Table S1). PNET (positive control), pancreatic neuroendocrine tumor; no SSTR2 antibodies (Ab), negative control; FTC, follicular thyroid cancer; PDTC, poorly DTC. **B,** Significantly higher ^{68}Ga-DOTA-TATE uptake in patients with HTC (14 metastatic lesions analyzed in 5 patients), compared with MTC (24 metastatic lesions analyzed in 8 patients) and PTC (36 metastatic lesions analyzed in 12 patients). **C,** ^{68}Ga-DOTA-TATE PET (black and white) and PET/CT (soft-tissue window) imaging in a patient with metastatic HTC (SUV_{max} ranging between 16.5 and 33). **D,** ^{68}Ga-DOTA-TATE PET/CT imaging in a patient with metastatic PTC (SUV_{max} ranging between 17.9 and 27.2). **E,** ^{68}Ga-DOTA-TATE PET/CT imaging in a patient with metastatic MTC with an intact thyroid (thyroid tumor uptake SUV_{max} ranging between 9.4 and 35.5).

results indicate that valproic acid treatment is associated with increased SSTR2 expression in thyroid cancer cells independent of baseline expression levels. Higher SSTR2 protein expression in valproic acid–treated cells is associated with increased H3ac and/or H4ac at the SSTR2 promoter.

^{86}Y-DOTA-EB-TATE is a superior SST analogue in the imaging of SSTR2-expressing tumors

The uptake of the radiolabeled SST analogues in FTC133, BCPAP, TT, and AR42J subcutaneous xenograft models was analyzed. Irrespective of the cell lines, ^{86}Y-DOTA-EB-TATE showed the highest tumor uptake in all mice models in comparison with ^{68}Ga-DOTA-TATE and ^{68}Ga-DOTA-JR11 (**Fig. 3A** and **C–E**; **Table 1**).

The uptake of ^{68}Ga-DOTA-TATE and ^{68}Ga-DOTA-JR11 was similar in all mice models (**Table 1**). Tumors derived from AR42J cells (high SSTR2 expression) showed the highest uptake among all SST analogues in comparison with FTC133, BCPAP, and MTC (TT) mice models ($P < 0.001$; **Fig. 3F**; **Table 1**).

In addition to the subcutaneous mice model, the uptake of three SST analogues was examined in a metastatic FTC133 mice model. Similar to the subcutaneous mouse model, ^{86}Y-DOTA-EB-TATE had the highest uptake in the metastatic lesions in comparison with ^{68}Ga-DOTA-TATE ($P < 0.001$) and ^{68}Ga-DOTA-JR11 ($P < 0.001$), respectively (**Fig. 3B**).

We next evaluated whether valproic acid treatment improved the uptake of SST analogues in the subcutaneous and metastatic mice models. Irrespective of the model, no significant effect from valproic acid treatment was observed on the uptake of the SST analogues (Supplementary Fig. S4A–S4D). However, IHC staining did reveal higher cytoplasmic SSTR2 expression in tumor tissues derived from mice exposed to valproic acid compared with placebo in FTC133 ($P = 0.023$) and AR42J ($P = 0.016$) models (Supplementary Table S3). Similar to valproic acid, decitabine treatment did not improve the uptake of ^{86}Y-DOTA-EB-TATE in FTC133 and AR42J subcutaneous mice models, as indicated by PET scans (Supplementary Fig. S5A and S5B).

The alternative to the upregulation of SSTR2 *in vivo* is to utilize SST analogues possessing the highest binding affinity and diagnostic and therapeutic activity. Significantly enhanced tumor uptake could be obtained by using the SST analogue ^{86}Y-DOTA-EB-TATE compared with ^{68}Ga-DOTA-TATE ($P < 0.001$) and ^{68}Ga-DOTA-JR11 ($P < 0.001$).

High SSTR2–expressing tumors are characterized by enhanced uptake of an SST analogue

To determine and compare the uptake of radiolabeled SST analogue by normal body organs and tumor tissue, biodistribution studies were performed on FTC133 and AR42J tumor–bearing mice after

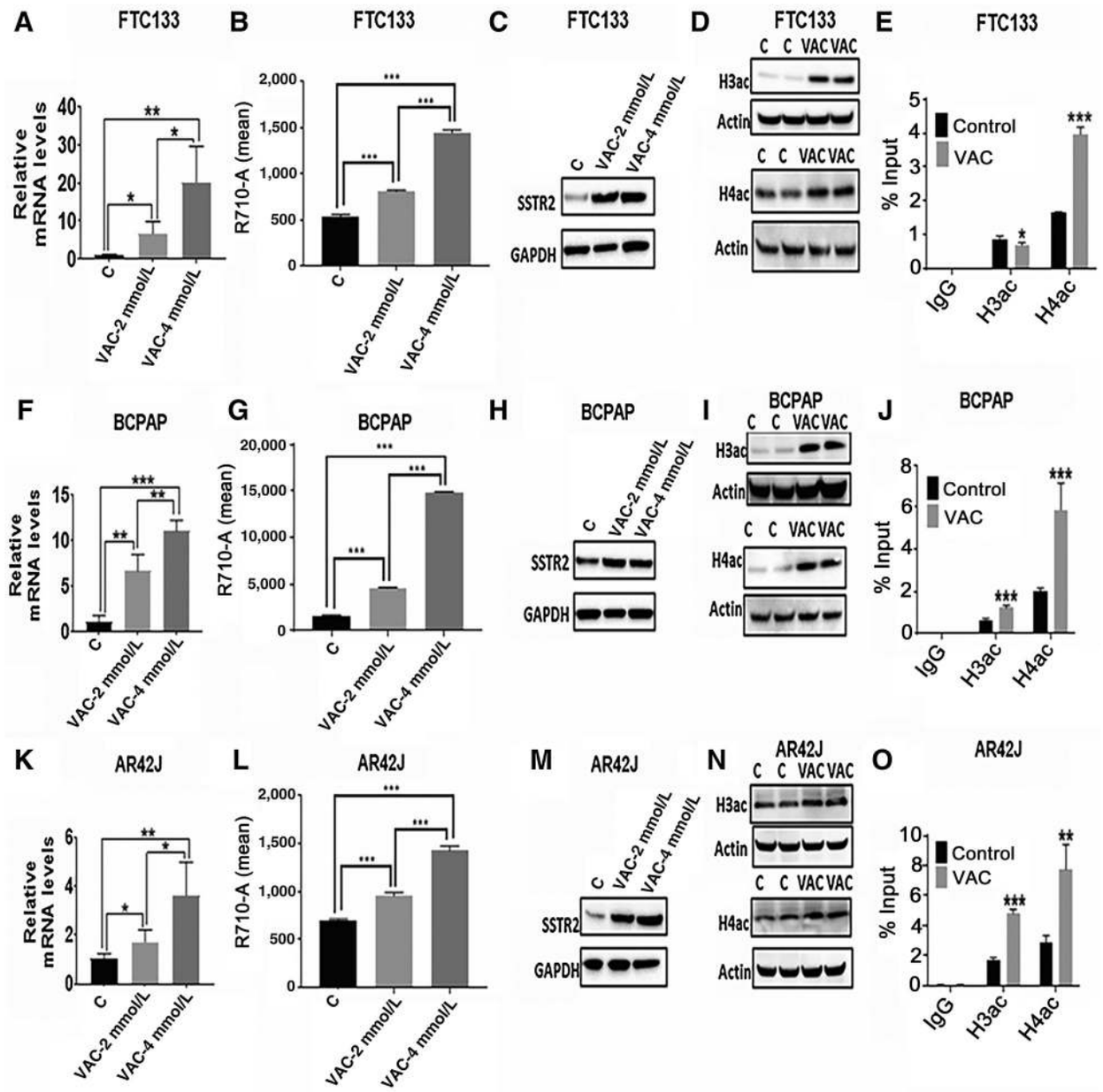

Figure 2.

Valproic acid–associated increased histone acetylation is associated with higher SSTR2 expression in thyroid cancer cells. **A**, **F**, and **K,** An increase in *SSTR2* mRNA expression in FTC133 ($n = 4$), BCPAP ($n = 4$), and AR42J cells ($n = 4$) upon valproic acid (VAC) treatment (2 and 4 mmol/L; 72 hours). ***, $P < 0.001$; **, $P < 0.01$; *, $P < 0.05$. C, control. **B**, **G**, and **L,** An increase in surface expression of SSTR2 expression in FTC133 ($n = 3$), BCPAP ($n = 3$), and AR42J cells ($n = 3$) upon valproic acid treatment (2 and 4 mmol/L; 72 hours). ***, $P < 0.001$. C, control. **C**, **H**, and **M,** An increase in SSTR2 protein expression in FTC133 ($n = 3$), BCPAP ($n = 3$), and AR42J cells ($n = 3$) upon valproic acid treatment (2 and 4 mmol/L; 72 hours). C, control. **D**, **I**, and **N,** An increase in global histone acetylation (H3ac and H4ac) at the protein level in FTC133 ($n = 3$), BCPAP ($n = 3$), and AR42J cells ($n = 3$) upon valproic acid treatment (4 mmol/L; 72 hours). C, control. **E**, **J**, and **O,** An increase in the amount of H4ac at the *SSTR2* promoter in FTC133 ($n = 4$), BCPAP ($n = 4$), and AR42J cells ($n = 4$) upon valproic acid treatment (4 mmol/L; 72 hours). An increase in the amount of H3ac at the *SSTR2* promoter observed in BCPAP ($n = 4$) and AR42J cells ($n = 4$) upon valproic acid treatment (4 mmol/L). ***, $P < 0.001$; **, $P < 0.01$; *, $P < 0.05$ with respect to control. C, control. Data are presented as mean ± SD. The SSTR2 antibodies used in the study had a lower affinity for rat than human SSTR2 epitope leading to weak signals despite very high SST analogue uptake in AR42J cells.

^{86}Y-DOTA-EB-TATE scans. In FTC133 mice, the uptake by tumor tissue (5.8 ± 0.8 %ID/g) was comparable with the spleen (5.1 ± 3.5 %ID/g; $P = 0.7$), while the liver (4.24 ± 0.43 %ID/g; $P < 0.01$) and heart (3.76 ± 0.7 %ID/g; $P < 0.01$) had significantly lower uptake compared with tumor tissue. In contrast, uptake by the kidneys (11.6 ± 1.1 %ID/g; $P < 0.001$) and lungs (8.5 ± 1.4 %ID/g; $P < 0.01$) was significantly higher than FTC133 tumors (**Fig. 4A**). In AR42J tumor–bearing mice, tumor uptake (19.13 ± 8.8 %ID/g) was

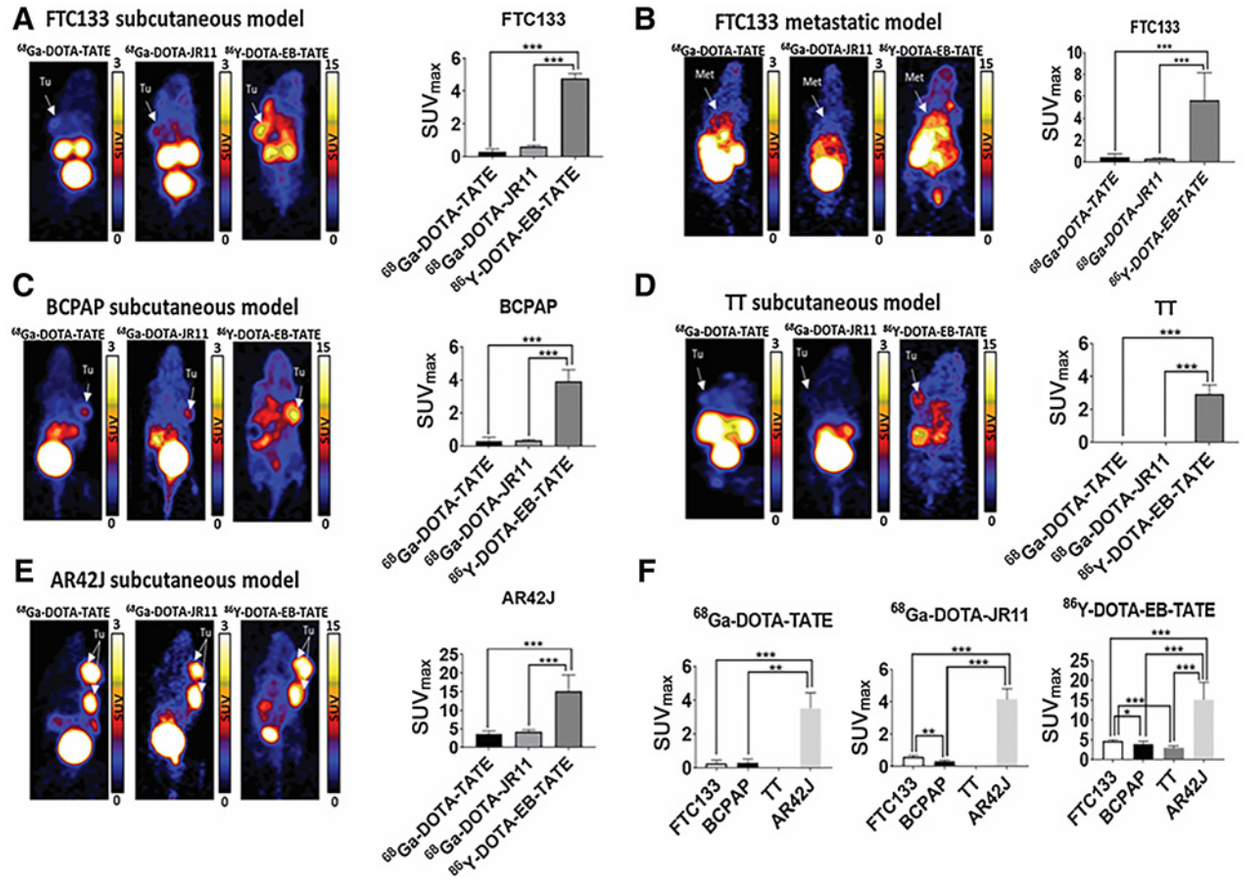

Figure 3.

DOTA-EB-TATE is a superior SST analogue in comparison with DOTA-TATE and DOTA-JR11. High SSTR2–expressing AR42J tumors are characterized by superior uptake of SST analogues compared with low SSTR2–expressing FTC133, BCPAP, and TT tumors. **A,** Representative PET images comparing uptake of ^{68}Ga-DOTA-TATE, ^{68}Ga-DOTA-JR11, and ^{86}Y-DOTA-EB-TATE in FTC133 subcutaneous xenograft mice model. The bar graph shows a significantly higher uptake of ^{86}Y-DOTA-EB-TATE in comparison with ^{68}Ga-DOTA-TATE and ^{68}Ga-DOTA-JR11 in FTC133 ($n = 5$) subcutaneous mice model. ***, $P < 0.001$. **B,** Representative PET images comparing uptake of ^{68}Ga-DOTA-TATE, ^{68}Ga-DOTA-JR11, and ^{86}Y-DOTA-EB-TATE in FTC133 metastatic mice model. The bar graph shows a significantly higher uptake of ^{86}Y-DOTA-EB-TATE in comparison with ^{68}Ga-DOTA-TATE and ^{68}Ga-DOTA-JR11 in FTC133 (n = 8–12) metastatic mice model. ***, $P < 0.001$. **C,** Representative PET images comparing the uptake of ^{68}Ga-DOTA-TATE, ^{68}Ga-DOTA-JR11, and ^{86}Y-DOTA-EB-TATE in BCPAP subcutaneous xenograft mice model. The bar graph shows a significantly higher uptake of ^{86}Y-DOTA-EB-TATE in comparison with ^{68}Ga-DOTA-TATE and ^{68}Ga-DOTA-JR11 in BCPAP ($n = 3$) subcutaneous mice model. ***, $P < 0.001$. **D,** Representative PET images comparing uptake of ^{68}Ga-DOTA-TATE, ^{68}Ga-DOTA-JR11, and ^{86}Y-DOTA-EB-TATE in TT subcutaneous xenograft mice model. The bar graph shows a significantly higher uptake of ^{86}Y-DOTA-EB-TATE in comparison with ^{68}Ga-DOTA-TATE and ^{68}Ga-DOTA-JR11 in TT ($n = 5$) subcutaneous mice model. ***, $P < 0.001$. **E,** Representative PET images comparing uptake of ^{68}Ga-DOTA-TATE, ^{68}Ga-DOTA-JR11, and ^{86}Y-DOTA-EB-TATE in AR42J subcutaneous xenograft mice model. The bar graph shows a significantly higher uptake of ^{86}Y-DOTA-EB-TATE in comparison with ^{68}Ga-DOTA-TATE and ^{68}Ga-DOTA-JR11 in AR42J (n = 4) subcutaneous mice model. ***, $P < 0.001$. **F,** The bar graph compares FTC133 ($n = 5$), BCPAP ($n = 3$), TT ($n = 5$), and AR42J ($n = 4$) subcutaneous mice models for the uptake of ^{68}Ga-DOTA-TATE, ^{68}Ga-DOTA-JR11, and ^{86}Y-DOTA-EB-TATE. ^{86}Y-DOTA-EB-TATE has the highest uptake in comparison with ^{68}Ga-DOTA-TATE and ^{68}Ga-DOTA-JR11 in all the mice models. *, $P < 0.05$; **, $P < 0.01$; ***, $P < 0.001$. Tumors (Tu) and metastasis (Met) are indicated by white arrows. The SUV scales range from 0 to 3 for ^{68}Ga-DOTA-TATE and ^{68}Ga-DOTA-JR11, and 0 to 15 for ^{86}Y-DOTA-EB-TATE. Data are presented as mean ± SD.

superior to the uptake by the liver (2.4 ± 0.56 %ID/g; $P < 0.01$), kidneys (6.9 ± 1.5 %ID/g; $P < 0.05$), spleen (2.2 ± 0.8 %ID/g; $P < 0.01$), heart (2.4 ± 0.36 %ID/g; $P < 0.01$), and lungs (5.4 ± 1 %ID/g; $P < 0.05$; **Fig. 4D**). Similar to PET imaging, biodistribution analysis also revealed superior uptake by AR42J tumors (3.3-fold higher; $P < 0.05$) in comparison with FTC133 tumors. Moreover, as expected, higher uptake of ^{86}Y-DOTA-EB-TATE by AR42J tumors was associated with relatively reduced uptake by normal organs in comparison with the FTC133 mice model. Neither valproic acid nor decitabine treatment resulted in any significant difference in the uptake of ^{86}Y-DOTA-EB-TATE within the tumor and normal tissues in comparison with the control mice (Supplementary Fig. S6A–S6D).

^{177}Lu-DOTA-EB-TATE therapy promotes tumor regression and improves disease-specific survival in high SSTR2–expressing tumors

Because DOTA-EB-TATE had the highest uptake in tumor tissues, therapeutic efficacy of this analogue radiolabeled with ^{177}Lu (half-life 6.7 days) was tested in high SSTR2–expressing (AR42J) and low SSTR2–expressing tumors (FTC133). After receiving the first dose of ^{177}Lu-DOTA-EB-TATE, AR42J tumors were stabilized and did not

Table 1. Comparison of the SUV_{max} of radiolabeled SST analogues in FTC133, BCPAP, TT, and AR42J subcutaneous xenograft mice models.

	Uptake of radiolabeled SST analogues ($SUV_{max} \pm SD$)			*P*		
Cell lines	^{68}Ga-DOTA-TATE	^{68}Ga-DOTA-JR11	^{86}Y-DOTA-EB-TATE	^{68}Ga-DOTA-TATE vs. ^{68}Ga-DOTA-JR11	^{68}Ga-DOTA-TATE vs. ^{68}Ga-DOTA-EB-TATE	^{68}Ga-DOTA-JR11 vs. ^{68}Ga-DOTA-EB-TATE
FTC133	0.28 ± 0.19	0.59 ± 0.1	4.8 ± 0.27	0.0668	<0.0001	<0.0001
BCPAP	0.28 ± 0.25	0.34 ± 0.06	3.92 ± 0.7	0.985	0.0001	0.0001
TT	0 ± 0	0 ± 0	2.94 ± 0.55	>0.9999	<0.0001	<0.0001
AR42J	3.53 ± 0.91	4.14 ± 0.65	15.16 ± 4.34	0.9407	0.0003	0.0005

progress further in size. After receiving a second dose 1 week later, these mice showed a decline in tumor growth. In contrast, the tumors of placebo-treated mice continued to progress, and the mice had to be euthanized within 14 days (**Fig. 4E** and **F**). The disease-specific survival of the mice that received ^{177}Lu-DOTA-EB-TATE therapy was significantly higher than the control group ($P < 0.001$). In contrast, the low SSTR2–expressing FTC133 tumors did not respond to the ^{177}Lu-DOTA-EB-TATE treatment (**Fig. 4B** and **C**). Valproic acid pretreatment did not improve the efficacy of ^{177}Lu-DOTA-EB-TATE in either AR42J or FTC133 mice models (Supplementary Fig. S7A and S7B).

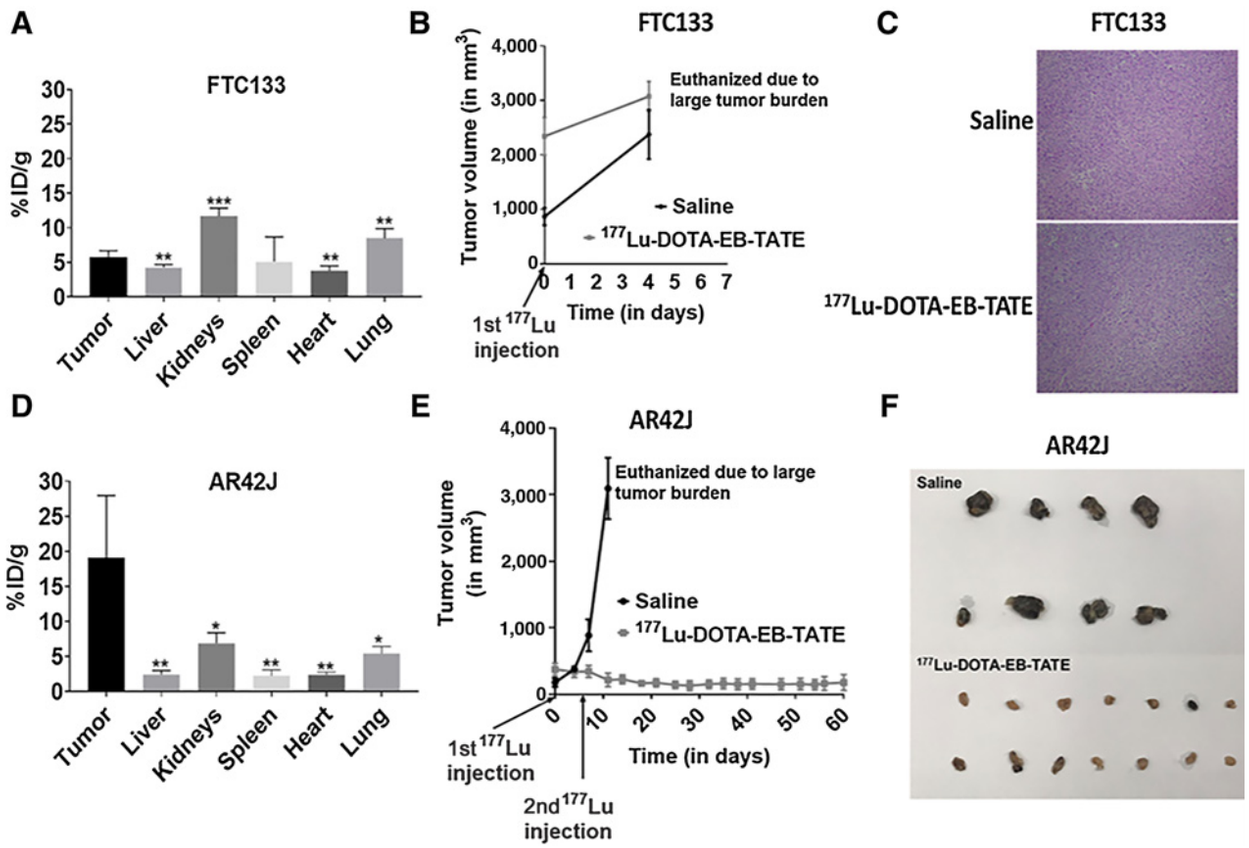

Figure 4.

Treatment with DOTA-EB-TATE promotes tumor regression and PFS in high SSTR2–expressing tumors. **A,** The bar graph shows quantification of ^{86}Y-DOTA-EB-TATE in the tumor and normal tissues (liver, kidneys, spleen, heart, and lungs) of the FTC133 subcutaneous xenograft mice ($n = 5$). ***, $P < 0.001$; **, $P < 0.01$ with respect to tumor tissue. **B,** No effect of PRRT on FTC133 (low SSTR2 expressing) subcutaneous xenograft mice receiving ^{177}Lu-DOTA-EB-TATE treatment ($n = 8$) in comparison with the mice that received saline ($n = 4$). Data are presented as mean ± SEM. **C,** Representative hematoxylin and eosine–stained slides show no difference in the histology of FTC133 tumors derived from the saline- and ^{177}Lu-DOTA-EB-TATE–treated mice. **D,** The bar graph shows quantification of ^{86}Y-DOTA-EB-TATE in the tumor and normal tissues (liver, kidneys, spleen, heart, and lungs) of the AR42J subcutaneous xenograft mice ($n = 4$). **, $P < 0.01$; *, $P < 0.05$ with respect to tumor tissue. **E,** Significant reduction in the tumor volume of the AR42J (high SSTR2 expressing) subcutaneous xenograft mice that received ^{177}Lu-DOTA-EB-TATE treatment ($n = 8$) in comparison with the saline-treated mice ($n = 4$). Data are presented as mean ± SEM. **F,** Representative images of the tumor tissues collected after euthanasia from saline- and ^{177}Lu-DOTA-EB-TATE–treated AR42J subcutaneous xenograft mice.

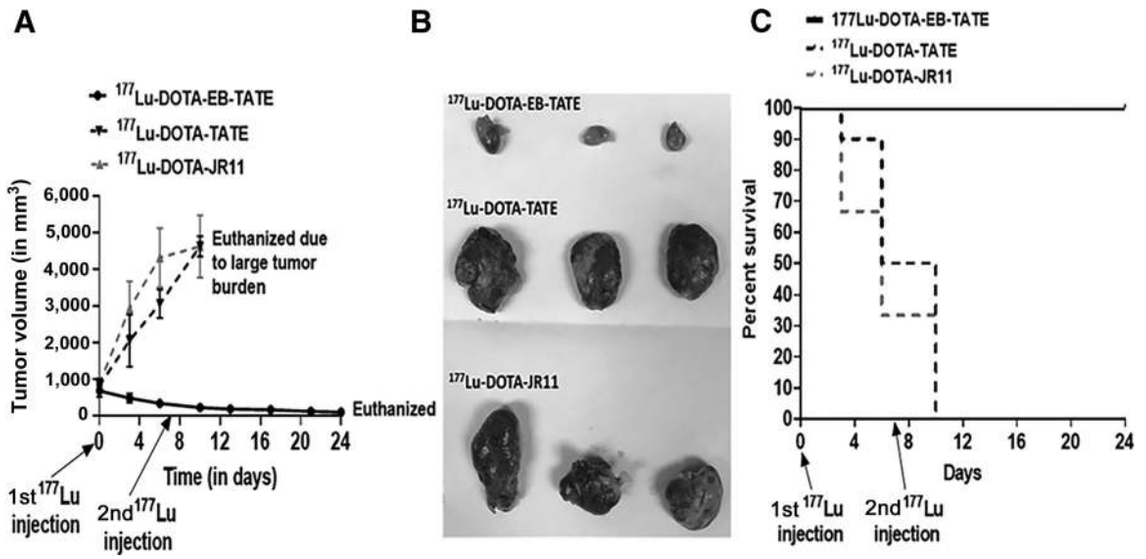

Figure 5.

DOTA-EB-TATE is a superior SST analogue in the treatment of SSTR2-expressing tumors. **A,** Significant reduction in the tumor volume of the AR42J subcutaneous mice model on treatment with ^{177}Lu-DOTA-EB-TATE ($n = 9$) in comparison with the ^{177}Lu-DOTA-TATE ($n = 10$) and ^{177}Lu-DOTA-JR11 ($n = 9$). Data are presented as mean ± SEM. **B,** Representative images of the tumor tissues collected after euthanasia from ^{177}Lu-DOTA-EB-TATE–, ^{177}Lu-DOTA-TATE–, ^{177}Lu-DOTA-JR11–treated AR42J subcutaneous xenograft mice. **C,** Kaplan–Meier survival curve comparing disease-specific survival (DSS) among different SST analogues in AR42J subcutaneous xenograft mice. The graph depicts significantly longer DSS of the ^{177}Lu-DOTA-EB-TATE–treated mice in comparison with ^{177}Lu-DOTA-TATE– and ^{177}Lu-DOTA-JR11–treated mice.

The therapeutic efficacy of all three SST analogues was compared in the AR42J mice model. Consistent with the observed higher tumor uptake on imaging, ^{177}Lu-DOTA-EB-TATE–treated mice responded to treatment, with an overall 87% ± 13% reduction in the tumor volume after 2 weeks (**Fig. 5A** and **B**). In contrast, mice treated with ^{177}Lu-DOTA-TATE and ^{177}Lu-DOTA-JR11 showed continued tumor progression and had to be euthanized within 10 days after the starting therapy (**Fig. 5A** and **B**). The disease-specific survival in the ^{177}Lu-DOTA-EB-TATE–treated mice (24 ± 0 days) was significantly longer compared with ^{177}Lu-DOTA-TATE– (7.7 ± 2.6 days; $P < 0.001$) and ^{177}Lu-DOTA-JR11–treated mice (6.3 ± 3 days; $P < 0.001$) (**Fig. 5C**). There was no difference in disease-specific survival between ^{177}Lu-DOTA-TATE– and ^{177}Lu-DOTA-JR11–treated mice ($P = 0.3$; **Fig. 5C**). Thus, ^{177}Lu-DOTA-EB-TATE is characterized by superior therapeutic efficacy in the management of tumors with high SSTR2 expression. None of the radiolabeled SST analogues were effective in tumors with low-to-moderate SSTR2 expression.

Discussion

We demonstrated that SSTR2 may serve as a molecular target in the diagnosis and treatment of a subset of patients with thyroid cancer. First, we showed that patients with HTC are characterized by high ^{68}Ga-DOTA-TATE uptake. As SUV_{max} of >13–15 has been associated with improved objective response rate and extended progression-free survival (PFS) in patients with neuroendocrine tumors, the median SUV_{max} of 16.5 (7.9–29) observed in patients with HTC suggests that PRRT might be beneficial in these patients, which are currently lacking effective therapeutic options (26–29). Further supporting this observation is our *in vivo* AR42J model, characterized by average EB-TATE SUV_{max} of 15.16 ± 4.34 in the tumor tissue, that responded to therapy with ^{177}Lu-EB-TATE with a significant reduction in tumor size and extended survival. In contrast, FTC133 *in vivo* model with a low radiolabeled analogue SUV_{max} of 4.8 ± 0.27 did not respond to PRRT.

Currently, there are a few small-scale studies showing promising results for the treatment of patients with RAI non-avid thyroid cancer with radiolabeled SST analogues (30–32). In a study of 16 patients with RAI non-avid progressive thyroid cancer (eight DTCs and eight MTCs), treatment with ^{90}Yttrium (^{90}Y)- and/or ^{177}Lu-labeled DOTA-TATE resulted in mean overall survival (OS) of 4.2 years (95% confidence interval, 2.9–5.5) and median PFS of 25 months after initial PRRT (30). Versari and colleagues documented positive ^{68}Ga-DOTA-TOC uptake in 24 of 41 patients with progressive RAI-negative DTC and 11 patients treated with PRRT (^{90}Y-DOTA-TOC), showing an objective response rate of 63% with a response duration of 3.5–11.5 months (32). However, PRRT utilizing ^{90}Y has been associated with nephrotoxicity, which could be decreased by utilizing ^{177}Lu for radiolabeling (33). In contrary to these studies, ^{177}Lu-DOTA-TATE therapy of 5 patients with radioiodine-refractory DTC showed heterogeneous response despite good ^{68}Ga-DOTA-TATE uptake in the pretherapeutic PET scan (34). In our study, we showed that only a subset of patients with thyroid cancer had high uptake of radiolabeled SST analogues and may potentially benefit from PRRT. Therefore, we investigated potential ways to upregulate SSTR2 in preclinical models and tested SST analogues characterized by different binding capacities and pharmacokinetics.

SSTR2 expression has been shown to be regulated by epigenetic modulators (21, 35–38). We screened three epigenetic regulators of SSTR2 expression and utilized the most potent among them—HDAC inhibitor, valproic acid, which is commonly used for the treatment of epilepsy and shown to have an excellent safety profile (39). We showed that valproic acid increases SSTR2 expression in thyroid cancer cell lines *in vitro*, which is associated with increased H3ac and H4ac at the

SSTR2 promoter region. Unfortunately, we did not observe a significant valproic acid–induced increase in the uptake of SST analogues *in vivo*. Although valproic acid upregulated SSTR2 expression in the tumor tissues of the subcutaneous FTC133 and AR42J models, this increase in expression might be insufficient and characterized by a lack of increased localization of SSTR2 on the cell surface. In the future, it will be interesting to test more tumor-specific epigenetic regulators to improve SSTR2 expression on the cancer cell surface.

Our study is the first to test novel SST analogues, DOTA-EB-TATE and DOTA-JR11, in thyroid cancer, demonstrating that DOTA-EB-TATE is a superior SST agonist. We compared the SUV of the three analogues in each mouse serving as their own control and observed that DOTA-EB-TATE was characterized by enhanced SUV compared with DOTA-TATE and DOTA-JR11. We also compared the therapeutic efficacy of ^{177}Lu-labeled DOTA-TATE, DOTA-JR11, and DOTA-EB-TATE, documenting the superiority of the latter in the mouse model characterized by high SSTR2 expression. There are several studies that suggested the superiority of SST antagonists over SST agonists (16, 40, 41). In our study, no significant difference was observed in the uptake of octreotate (TATE agonist) versus JR11 (antagonist) linked to the same chelator (DOTA) in the tested mice models. However, attachment of Evans blue moiety to octreotate improved the uptake significantly. The addition of Evans blue moiety to the octreotate significantly improved its pharmacokinetics, as indicated by the increased half-life in the blood, lower clearance rate, and better tumor-to-organ uptake ratio (13, 14). In a recent study performed on 33 patients with metastatic neuroendocrine tumors, ^{177}Lu-DOTA-EB-TATE was observed to be more effective than similar dose of ^{177}Lu-DOTA-TATE (42). However, the study endpoint was a change in SUV before and after treatment, so there was no data on the effects on standardized hard endpoints, such as response rate by RECIST criteria, PFS, and OS. A possible concern regarding the use of DOTA-EB-TATE is that its enhanced binding to the albumin, and slow clearance rate will not only expose the tumor tissues, but also the healthy organs to the higher radiation doses. A study analyzing the safety profile of this agent reported that in comparison with ^{177}Lu-DOTA-TATE, the effective dose of ^{177}Lu-DOTA-EB-TATE was significantly higher in the kidneys and red bone marrow of the patients with metastatic neuroendocrine tumor (14). Although the small-scale pilot studies performed on patients with metastatic neuroendocrine tumors showed that ^{177}Lu-DOTA-EB-TATE is well tolerated by the patients at low doses without causing any significant hematotoxicity or nephrotoxicity (42, 43), more studies are necessary to understand the short- and long-term toxicity profile of this agent.

The major strength of our study is its translational relevance, as therapeutic efficacy of PRRT has been proven only for the model characterized by a high SSTR2 analogues uptake. It suggests that the tumors characterized by a high SUV_{max}, within 15.16 ± 4.34 range, may respond to PRRT using ^{177}Lu-DOTA-EB-TATE, while the uptake within SUV_{max} of 4.8 ± 0.27 is likely not going to translate into clinical efficacy.

Our study had a few limitations. We utilized non-thyroid cancer AR42J xenografts to model a high SUV of SST analogues, resembling SUV_{max} observed in our clinical trial in patients with HTC, as all screened thyroid cancer cell lines were characterized by low-to-moderate uptake of SST analogues *in vivo*. Nonetheless, testing radiolabeled SST analogues in models with differential SSTR2 expression levels revealed that the therapeutic efficacy of PRRT is achieved only in tumors with high SST analogues uptake.

In conclusion, our preclinical data document that DOTA-EB-TATE is a superior analogue over DOTA-TATE and DOTA-JR11 for the imaging and treatment of SSTR2-high–expressing tumors. A high ^{68}Ga-DOTA-TATE uptake observed in metastatic HTC makes these patients, who lack alternative treatment options, ideal candidates for PRRT. Our study forms a basis for a clinical trial testing the diagnostic and therapeutic efficacy of ^{177}Lu-DOTA-EB-TATE in patients with tumors characterized by high SST analogue uptake.

Authors' Disclosures

O. Jacobson reports a patent for chemical conjugates of Evans blue derivatives and their use as radiotherapy and imaging agents licensed and with royalties paid from E-150-2016-0-US-01. X. Chen reports a patent for WO2017196806A1 pending, licensed, and with royalties paid from Molecular Targeted Therapeutics, Inc. No disclosures were reported by the other authors.

Authors' Contributions

S. Thakur: Conceptualization, data curation, formal analysis, investigation, methodology, writing-original draft, writing-review and editing. **B. Daley:** Data curation, investigation, writing-review and editing. **C. Millo:** Data curation, software, formal analysis, writing-review and editing. **C. Cochran:** Resources, writing-review and editing. **O. Jacobson:** Data curation, software, formal analysis, methodology, writing-review and editing. **H. Lu:** Methodology, writing-review and editing. **Z. Wang:** Methodology, writing-review and editing. **D. Kiesewetter:** Resources, writing-review and editing. **X. Chen:** Resources, writing-review and editing. **V. Vasko:** Data curation, formal analysis, methodology, writing-review and editing. **J. Klubo-Gwiezdzinska:** Conceptualization, resources, data curation, formal analysis, supervision, funding acquisition, investigation, visualization, methodology, writing-original draft, project administration, writing-review and editing.

Acknowledgments

This work was supported by NIH/NIDDK Intramural funding ZIA DK 07513803. We thank our patients for participation in the study. We thank IPSEN for providing DOTA-JR11 for the animal studies. Special thanks to Dr. Peter Herscovitch, Chief of Positron Emission Tomography for supporting the clinical part of the study. Special thanks to Drs. Hongxiu Luo and Shirisha Avadhanula for seeing and coordinating care for a subset of study participants. Special thanks to flow cytometry core facility, National Heart, Lung, and Blood Institute, NIH for their help with flow cytometer experiments. We thank Drs. Lee S. Weinstein and Sunita Agarwal for a critical review of the article. We thank Sungyoung Auh for the statistical analysis of the data in relation to a reviewer's comment.

The costs of publication of this article were defrayed in part by the payment of page charges. This article must therefore be hereby marked *advertisement* in accordance with 18 U.S.C. Section 1734 solely to indicate this fact.

Received September 1, 2020; revised November 6, 2020; accepted December 15, 2020; published first December 22, 2020.

References

1. Wells SA Jr, Asa SL, Dralle H, Elisei R, Evans DB, Gagel RF, et al. Revised American Thyroid Association guidelines for the management of medullary thyroid carcinoma. Thyroid. 2015;25:567–610.
2. Dadu R, Cabanillas ME. Optimizing therapy for radioactive iodine-refractory differentiated thyroid cancer: current state of the art and future directions. Minerva Endocrinol 2012;37:335–56.

3. Besic N, Vidergar-Kralj B, Frkovic-Grazio S, Movrin-Stanovnik T, Auersperg M. The role of radioactive iodine in the treatment of Hurthle cell carcinoma of the thyroid. Thyroid 2003;13:577–84.
4. Durante C, Haddy N, Baudin E, Leboulleux S, Hartl D, Travagli JP, et al. Long-term outcome of 444 patients with distant metastases from papillary and follicular thyroid carcinoma: benefits and limits of radioiodine therapy. J Clin Endocrinol Metab 2006;91:2892–9.
5. Robbins RJ, Wan Q, Grewal RK, Reibke R, Gonen M, Strauss HW, et al. Real-time prognosis for metastatic thyroid carcinoma based on 2-[18F]fluoro-2-deoxy-D-glucose-positron emission tomography scanning. J Clin Endocrinol Metab 2006; 91:498–505.
6. Frank-Raue K, Machens A, Leidig-Bruckner G, Rondot S, Haag C, Schulze E, et al. Prevalence and clinical spectrum of nonsecretory medullary thyroid carcinoma in a series of 839 patients with sporadic medullary thyroid carcinoma. Thyroid 2013;23:294–300.
7. Weckbecker G, Lewis I, Albert R, Schmid HA, Hoyer D, Bruns C. Opportunities in somatostatin research: biological, chemical and therapeutic aspects. Nat Rev Drug Discov 2003;2:999–1017.
8. De Jong M, Valkema R, Jamar F, Kvols LK, Kwekkeboom DJ, Breeman WA, et al. Somatostatin receptor-targeted radionuclide therapy of tumors: preclinical and clinical findings. Semin Nucl Med 2002;32:133–40.
9. Sun LC, Coy DH. Somatostatin receptor-targeted anti-cancer therapy. Curr Drug Deliv 2011;8:2–10.
10. Hennrich U, Benesova M. [^{68}Ga]Ga-DOTA-TOC: the first FDA-approved ^{68}Ga-radiopharmaceutical for PET imaging. Pharmaceuticals 2020;13:38.
11. Raj N, Reidy-Lagunes D. The role of ^{68}Ga-DOTATATE positron emission tomography/computed tomography in well-differentiated neuroendocrine tumors: a case-based approach illustrates potential benefits and challenges. Pancreas 2018;47:1–5.
12. Maqsood MH, Tameez Ud Din A, Khan AH. Neuroendocrine tumor therapy with lutetium-177: a literature review. Cureus 2019;11:e3986.
13. Tian R, Jacobson O, Niu G, Kiesewetter DO, Wang Z, Zhu G, et al. Evans blue attachment enhances somatostatin receptor subtype-2 imaging and radiotherapy. Theranostics 2018;8:735–45.
14. Zhang J, Wang H, Jacobson O, Cheng Y, Niu G, Li F, et al. Safety, pharmacokinetics, and dosimetry of a long-acting radiolabeled somatostatin analog (177)Lu-DOTA-EB-TATE in patients with advanced metastatic neuroendocrine tumors. J Nucl Med 2018;59:1699–705.
15. Fani M, Nicolas GP, Wild D. Somatostatin receptor antagonists for imaging and therapy. J Nucl Med 2017;58:61s–6s.
16. Ginj M, Zhang H, Waser B, Cescato R, Wild D, Wang X, et al. Radiolabeled somatostatin receptor antagonists are preferable to agonists for *in vivo* peptide receptor targeting of tumors. Proc Natl Acad Sci U S A 2006;103:16436–41.
17. Dalm SU, Nonnekens J, Doeswijk GN, de Blois E, van Gent DC, Konijnenberg MW, et al. Comparison of the therapeutic response to treatment with a 177Lu-labeled somatostatin receptor agonist and antagonist in preclinical models. J Nucl Med 2016;57:260–5.
18. Nicolas GP, Schreiter N, Kaul F, Uiters J, Bouterfa H, Kaufmann J, et al. Sensitivity comparison of (68)Ga-OPS202 and (68)Ga-DOTATOC PET/CT in patients with gastroenteropancreatic neuroendocrine tumors: a prospective phase II imaging study. J Nucl Med 2018;59:915–21.
19. Nockel P, Millo C, Keutgen X, Klubo-Gwiezdzinska J, Shell J, Patel D, et al. The rate and clinical significance of incidental thyroid uptake as detected by gallium-68 DOTATATE positron emission tomography/computed tomography. Thyroid 2016;26:831–5.
20. Chang CA, Pattison DA, Tothill RW, Kong G, Akhurst TJ, Hicks RJ, et al. ^{68}Ga-DOTATATE and ^{18}F-FDG PET/CT in paraganglioma and pheochromocytoma: utility, patterns and heterogeneity. Cancer Imaging 2016;16:22.
21. Taelman VF, Radojewski P, Marincek N, Ben-Shlomo A, Grotzky A, Olariu CI, et al. Upregulation of key molecules for targeted imaging and therapy. J Nucl Med 2016;57:1805–10.
22. Harvey JM, Clark GM, Osborne CK, Allred DC. Estrogen receptor status by immunohistochemistry is superior to the ligand-binding assay for predicting response to adjuvant endocrine therapy in breast cancer. J Clin Oncol 1999;17: 1474–81.
23. Zhang L, Gaskins K, Yu Z, Xiong Y, Merino MJ, Kebebew E. An *in vivo* mouse model of metastatic human thyroid cancer. Thyroid 2014;24:695–704.
24. Zhang L, Vines DC, Scollard DA, McKee T, Komal T, Ganguly M, et al. Correlation of somatostatin receptor-2 expression with gallium-68-DOTA-TATE uptake in neuroblastoma xenograft models. Contrast Media Mol Imaging 2017;2017:9481276.
25. Cancer Genome Atlas Research Network. Integrated genomic characterization of papillary thyroid carcinoma. Cell 2014;159:676–90.
26. Sharma R, Wang WM, Yusuf S, Evans J, Ramaswami R, Wernig F, et al. ^{68}Ga-DOTATATE PET/CT parameters predict response to peptide receptor radionuclide therapy in neuroendocrine tumours. Radiother Oncol 2019;141:108–15.
27. Zhang J, Kulkarni HR, Singh A, Niepsch K, Müller D, Baum RP. Peptide receptor radionuclide therapy in grade 3 neuroendocrine neoplasms: safety and survival analysis in 69 patients. J Nucl Med 2019;60:377–85.
28. Kayani I, Bomanji JB, Groves A, Conway G, Gacinovic S, Win T, et al. Functional imaging of neuroendocrine tumors with combined PET/CT using ^{68}Ga-DOTATATE (DOTA-DPhe1, Tyr3-octreotate) and 18F-FDG. Cancer 2008;112:2447–55.
29. Mojtahedi A, Thamake S, Tworowska I, Ranganathan D, Delpassand ES. The value of ^{68}Ga-DOTATATE PET/CT in diagnosis and management of neuroendocrine tumors compared to current FDA approved imaging modalities: a review of literature. Am J Nucl Med Mol Imaging 2014;4:426–34.
30. Budiawan H, Salavati A, Kulkarni HR, Baum RP. Peptide receptor radionuclide therapy of treatment-refractory metastatic thyroid cancer using (90)Yttrium and (177)Lutetium labeled somatostatin analogs: toxicity, response and survival analysis. Am J Nucl Med Mol Imaging 2013;4:39–52.
31. Lapa C, Werner RA, Schmid JS, Papp L, Zsótér N, Biko J, et al. Prognostic value of positron emission tomography-assessed tumor heterogeneity in patients with thyroid cancer undergoing treatment with radiopeptide therapy. Nucl Med Biol 2015;42:349–54.
32. Versari A, Sollini M, Frasoldati A, Fraternali A, Filice A, Froio A, et al. Differentiated thyroid cancer: a new perspective with radiolabeled somatostatin analogues for imaging and treatment of patients. Thyroid 2014;24:715–26.
33. Alsadik S, Yusuf S, Al-Nahhas A. Peptide receptor radionuclide therapy for pancreatic neuroendocrine tumours. Curr Radiopharm 2019;12:126–34.
34. Roll W, Riemann B, Schafers M, Stegger L, Vrachimis A. ^{177}Lu-DOTATATE therapy in radioiodine-refractory differentiated thyroid cancer: a single center experience. Clin Nucl Med 2018;43:e346–e51.
35. Veenstra MJ, van Koetsveld PM, Dogan F, Farrell WE, Feelders RA, Lamberts SWJ, et al. Epidrug-induced upregulation of functional somatostatin type 2 receptors in human pancreatic neuroendocrine tumor cells. Oncotarget 2018;9: 14791–802.
36. Torrisani J, Hanoun N, Laurell H, Lopez F, Maoret JJ, Souque A, et al. Identification of an upstream promoter of the human somatostatin receptor, hSSTR2, which is controlled by epigenetic modifications. Endocrinology 2008; 149:3137–47.
37. Guenter RE, Aweda T, Carmona Matos DM, Whitt J, Chang AW, Cheng EY, et al. Pulmonary carcinoid surface receptor modulation using histone deacetylase inhibitors. Cancers 2019;11:767.
38. Jin XF, Auernhammer CJ, Ilhan H, Lindner S, Nolting S, Maurer J, et al. Combination of 5-fluorouracil with epigenetic modifiers induces radiosensitization, somatostatin receptor 2 expression, and radioligand binding in neuroendocrine tumor cells *in vitro*. J Nucl Med 2019;60:1240–6.
39. Trinka E, Hofler J, Zerbs A, Brigo F. Efficacy and safety of intravenous valproate for status epilepticus: a systematic review. CNS Drugs 2014;28:623–39.
40. Zhu W, Cheng Y, Wang X, Yao S, Jia R, Xu J, et al. Head-to-head comparison of ^{68}Ga-DOTA-JR11 and ^{68}Ga-DOTATATE PET/CT in patients with metastatic, well-differentiated neuroendocrine tumors: a prospective study. J Nucl Med 2019;61:897–903.
41. Wild D, Fani M, Fischer R, Del Pozzo L, Kaul F, Krebs S, et al. Comparison of somatostatin receptor agonist and antagonist for peptide receptor radionuclide therapy: a pilot study. J Nucl Med 2014;55:1248–52.
42. Liu Q, Cheng Y, Zang J, Sui H, Wang H, Jacobson O, et al. Dose escalation of an Evans blue-modified radiolabeled somatostatin analog ^{177}Lu-DOTA-EB-TATE in the treatment of metastatic neuroendocrine tumors. Eur J Nucl Med Mol Imaging 2020;47:947–57.
43. Wang H, Cheng Y, Zhang J, Zang J, Li H, Liu Q, et al. Response to single low-dose ^{177}Lu-DOTA-EB-TATE treatment in patients with advanced neuroendocrine neoplasm: a prospective pilot study. Theranostics 2018;8:3308–16.